Supporting Information

L-Cysteine Functionalized Magnetite Nanoparticles Adorned Ti_3C_2-MXene Nanohybrid based Screen Printed Immunosensor for Oral Cancer Biomarker Detection

Manali Choramle[1#], Damini Verma[2#], Ashish Kalkal[3,4*], Rangadhar Pradhan[5], Avdhesh Kumar Rai[6], Gopinath Packirisamy[1,2 *]

[1]Department of Biosciences and Bioengineering, Indian Institute of Technology Roorkee, Roorkee, Uttarakhand, 247667, India

[2]Centre for Nanotechnology, Indian Institute of Technology Roorkee, Roorkee, Uttarakhand, 247667, India

[3]Nanostructured system Laboratory, Department of Mechanical Engineering, University College London, London, WC1E 7JE, UK

[4]Wellcome/EPSRC Centre for Interventional and Surgical Sciences, University College London, London W1W7TS, UK

[5]iHub Divyasmapark, Technology Innovation Hub, Indian Institute of Technology Roorkee, Roorkee, Uttarakhand, India-247667

[6]DBT Centre for Molecular Biology and Cancer Research, Dr Bhubaneswar Borooah Cancer Institute (Tata Memorial Centre), Gopinath Nagar, A K Azad Road, Guwahati-781016

# Authors have contributed Equally

***Corresponding author:** Ashish Kalkal, Gopinath Packirisamy

Email ID: a.kalkal@ucl.ac.uk, gopi@bt.iitr.ac.in

S1 Chemicals and Reagents

1-(3-(dimethylamino) propyl)-3-ethylcarbodiimide hydrochloride (EDC), Hexaammineruthenium (III) Chloride [Ru $(NH_3)_6]^{3+}$ and N-hydroxysuccinimide (NHS) were sourced from Sigma Aldrich. CYFRA 21-1 biomarker and Anti-CYFRA 21-1 were procured from Ray Biotech. Sodium diphosphate anhydrous [Na_2HPO_4] and Sodium monophosphate [NaH_2PO_4] were bought from Fisher Scientific. NaCl and NaOH pellets were sourced from Himedia, India. Commercial gold-based screen-printed electrodes (GSPE) of 250AT series were procured from Metrohm DropSens. Ferric chloride and ferrous chloride were procured from Loba Chemie Pvt Ltd. Ti_3C_2 MXene was purchased from Nanochemazone. L-Cyst was purchased from Sisco Research Laboratories, India. All the chemicals utilized were of analytical grade and used without the necessity for additional purification steps. Sodium diphosphate dihydrate and sodium monophosphate were mixed to prepare a phosphate buffer solution (0.2 M PBS) for performing electrochemical studies. All solutions were made using distilled water (DI) with a resistivity of 18.2 MΩ cm and stored at 4 °C.

S2 Instrumentation

X-ray diffraction (XRD, Bruker D-8 Advance) was employed to analyze the phase and crystallinity of the synthesized L-Cyst@MNPs, Ti_3C_2 MXene, and L-Cyst@MNPs/Ti_3C_2 MXene nanohybrid. A monochromatic X-ray beam with Cu-Kα radiation (λ = 1.5406 Å) was utilized for spectrum recording. Morphological and structural properties of nanohybrid and fabricated electrodes were examined through scanning electron microscopy (SEM) [Zeiss Ultra Plus, Carl Zeiss, Germany] and high-resolution transmission electron microscopy (HRTEM) [JEOL JEM-2200 FS (Japan) instrument]. UV-Visible spectrophotometer (Lasany LI-2800) was employed to study the absorption properties of the L-Cyst@MNPs, Ti_3C_2 MXene, and L-Cyst@MNPs/Ti_3C_2 MXene nanohybrid. Fourier transform infrared (FTIR) spectroscopy (Agilent Cary 630) was utilized to analyze the functionalization of MNPs with L-Cyst and

amide bond formation after antibodies immobilization onto L-Cyst@MNPs/Ti_3C_2 MXene/GSPE electrode. The differential pulse voltammetry (DPV), electrochemical impedance spectroscopy (EIS) and cyclic voltammetry (CV) techniques were performed using an Autolab Potentiostat/Galvanostat (Electrochemical analyzer, Metrohm, The Netherlands). For these studies, GSPE having working electrode of gold (4 mm diameter), counter of platinum, and reference of silver were utilized. Freshly prepared 0.2 M PBS solution (pH 7.0) containing [Ru $(NH_3)_6]^{3+}$(5 mM) as a redox coupler was used as an electron mediator, while for EIS studies 5 mM $[Fe(CN)_6]^{3-/4-}$ redox probe was utilized.

S3 Stock and Volume Optimization

To achieve a smooth and uniform coating on the GSPE, selecting the appropriate stock concentration of L-Cyst@MNPs/Ti_3C_2-Mxene is essential.

For this study, we prepared various stock concentrations of L-Cyst@MNPs/Ti_3C_2-Mxene, including 1, 3, and 5 mg mL^{-1} in DI. It was noted that the maximum magnitude of DPV peak current was observed at 5 mg mL^{-1} concentration, as illustrated in **Fig.S1 (a)** by utilizing PBS buffer (0.2 M, pH 7.0) consisting of [Ru $(NH_3)_6]^{3+}$ as redox species. The observed phenomenon could potentially be attributed to enhanced electron transfer between the electrolyte solution containing [Ru $(NH_3)_6]^{3+}$ and the interface of electrode surface area due to structural realignment of the L-Cyst@MNPs/Ti_3C_2-Mxene at 5 mg mL^{-1}. However, at lower concentrations (1 and 3 mg mL^{-1}), it is possible that the proper orientation of L-Cyst@MNPs/Ti_3C_2-Mxene did not occur, resulting in a decrement of DPV peak current values. Moreover, too high concentration has led to aggregation, hinder dispersion, or cause instability, thereby decreasing current. Hence, 5 mg mL^{-1} stock concentration of L-Cyst@MNPs/Ti_3C_2-Mxene nanohybrid was utilized to fabricate the L-Cyst@MNPs/Ti_3C_2-Mxene/GSPE electrode using drop cast method. **Fig.S1 (b)** illustrates its dot graph.

Similarly, the next step involved was selecting the appropriate volume. The volume of L-Cyst@MNPs/Ti_3C_2-Mxene (3 µL, 5 µL, and 7 µL) was carefully drop-casted onto the GSPE working area. **Fig.S1 (c)** depicts the DPV peak current observed for each volume. The highest DPV peak current is achieved with 7 µL that resulted in rapid binding kinetics [1]. However, on further increasing volume above this, attributed to the thicker barrier layers formed at higher coating volumes, which subsequently limit the flow of electrons between the electrode surface and redox species. Also, at higher volume, overflowing of liquid to counter and reference electrode might interfere with electrochemical response. Thus, at a volume of 7 µL, the most favourable conditions were achieved, facilitating a faster flow of electrons. Consequently, a solution of 5 mg mL^{-1} of L-Cyst@MNPs/Ti_3C_2-Mxene nanohybrid with a volume of 7 µL was selected for the modification of GSPE for subsequent electrochemical studies. Additionally, the dot graph is depicted in **Fig.S1 (d)**.

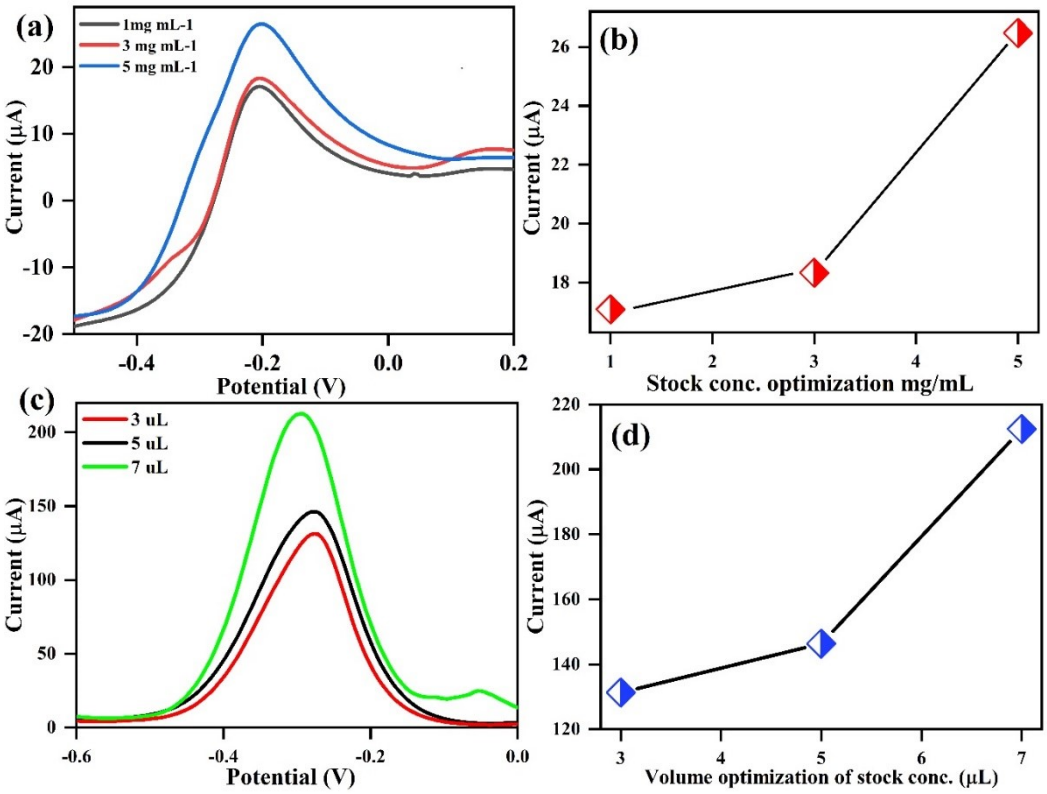

Fig. S1: (a) Stock concentration optimization of L-Cyst@MNPs/Ti_3C_2-Mxene nanohybrid, (b) Dot graph of stock concentration optimization, and (c) Volume optimization of L-Cyst@MNPs/Ti_3C_2-Mxene nanohybrid, (d) Dot graph of volume optimization

S4 Electrode Studies

EIS was further performed to observe the modification of various electrodes in PBS (0.2 M) comprising $[Fe(CN)_6]^{3-/4-}$ at 0 V from 100 kHz to 10 Hz frequency window. The variation in charge transfer resistance i.e., Rct value is depicted by Nyquist plot semicircle **[Fig. S2]** for various modified electrodes while the inset of **Fig.S2** showed equivalent circuit. The different parameters of Nyquist plot of bare GSPE (**Fig.S2, i**), Ti_3C_2-MXene/GSPE (**Fig.S2, ii**), L-Cyst@MNPs/GSPE (**Fig.S2, iii**), L-Cyst@MNPs/Ti_3C_2-MXene/GSPE (**Fig.S2, iv**), anti-CYFRA-21-1/L-Cyst@MNPs/Ti_3C_2-MXene/GSPE (**Fig.S2, v**), and BSA/anti-CYFRA-21-1/L-Cyst@MNPs/Ti_3C_2-MXene/GSPE (**Fig.S2, vi**) respectively, are illustrated in Table S1.

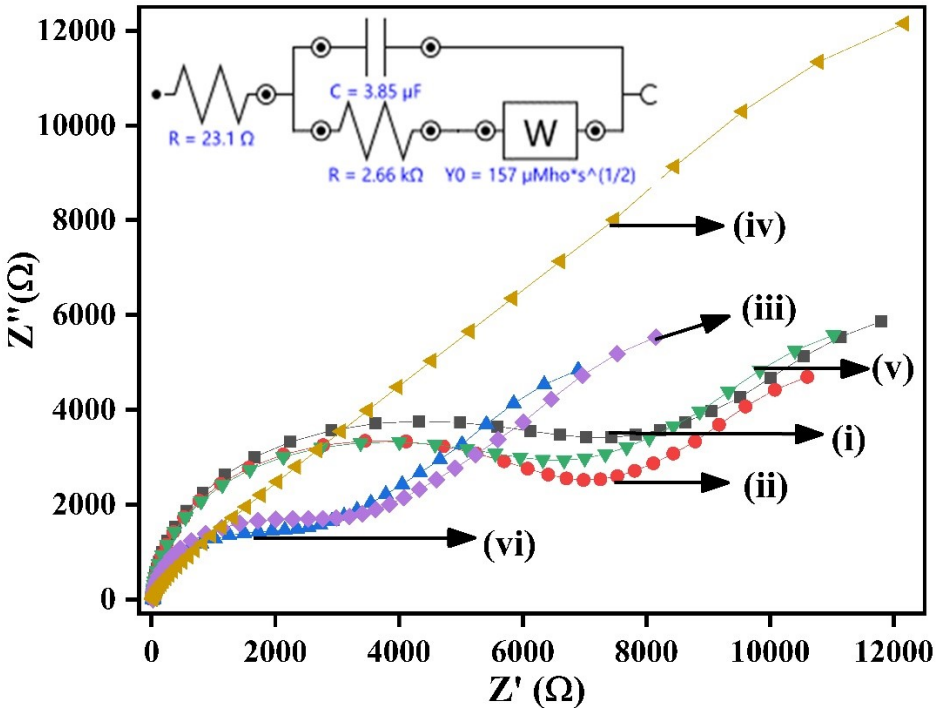

Fig.S2: EIS spectra of various electrodes namely (i) Bare GSPE (ii) Ti_3C_2-MXene/SPE (iii) L-Cyst@MNPs/GSPE (iv) L-Cyst@MNPs/Ti_3C_2-MXene/GSPE (v) anti-CYFRA-21-1/L-

Cyst@MNPs/Ti_3C_2-MXene/GSPE (vi) BSA/anti-CYFRA-21-1/L-Cyst@MNPs/Ti_3C_2 MXene/GSPE immunosensor

Table S1: Impedimetric characteristic of different modified electrodes

Electrodes	Charge transfer resistance Rct (KΩ)	Double-layer capacitance Cdl (µF)	Ohmic resistance Rs (Ω)	Warburg impedance Wz [µMho*s^(1/2)]
GSPE	6.44	2.62	24.7	155
Ti_3C_2-MXene/GSPE	6.1	3.35	22.1	190
L-Cyst@MNPsGSPE	2.66	3.85	23.1	157
L-Cyst@MNPs/Ti_3C_2-MXene/GSPE	3.61×10^{-3}	2.92	22.4	70
anti-CYFRA-21-1/L-Cyst@MNPs/Ti_3C_2-MXene/GSPE	5.77	4.15	23.2	160
BSA/anti-CYFRA-21-1/L-Cyst@MNPs/Ti_3C_2-MXene/GSPE	2.13	5.31	24.2	179

S5 Scan Rate Studies

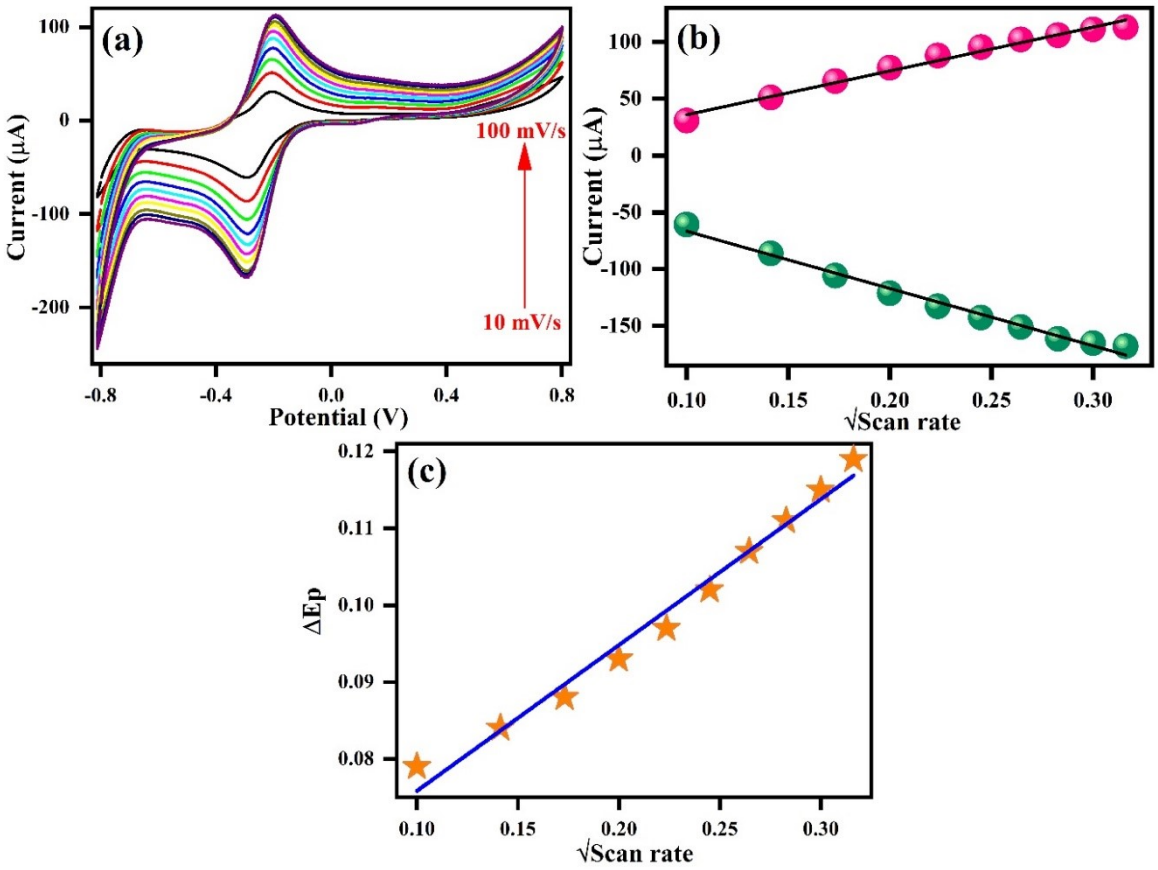

Fig. S3: (a) Scan Rate study of BSA/anti-CYFRA-21-1/L-cyst@MNPs/Ti_3C_2-MXene/GSPE (b) It shows the cathodic (Ip_c) and anodic (Ip_a) peak currents against √scan rate plot. (c) It shows the plot of differential peak potential (ΔE_p) and √scan rate.

Table S2: Enlist the calculated electrochemical attributes of the immunosensor.

Electrode/Material Used	**A_s (cm^2)**	**D ($cm^2\ s^{-1}$)**	**ΔEp (V)**	**K_s (s^{-1})**	**I* (mol cm^{-2})**
BSA/anti-CYFRA-21-1/L-Cyst@MNPs/Ti_3C_2 MXene/GSPE	0.125	5.47×10^{-12}	0.097	0.187	1.50×10^{-8}

S6 Electrochemical Response Studies

$$Sensitivity = \frac{slope}{area\ of\ immunosensor\ (0.125\ cm^2)} \quad \text{Eq. (S1)}$$

$$Limit\ of\ Quantification = \frac{10\sigma}{sensitivity} \quad \text{Eq. (S2)}$$

$$Limit\ of\ Detection = \frac{3\sigma}{sensitivity} \quad \text{Eq. (S3)}$$

where σ is the standard deviation (SD) of the immunosensor' intercept.

S7 Interferents, Reproducibility and Stability Studies

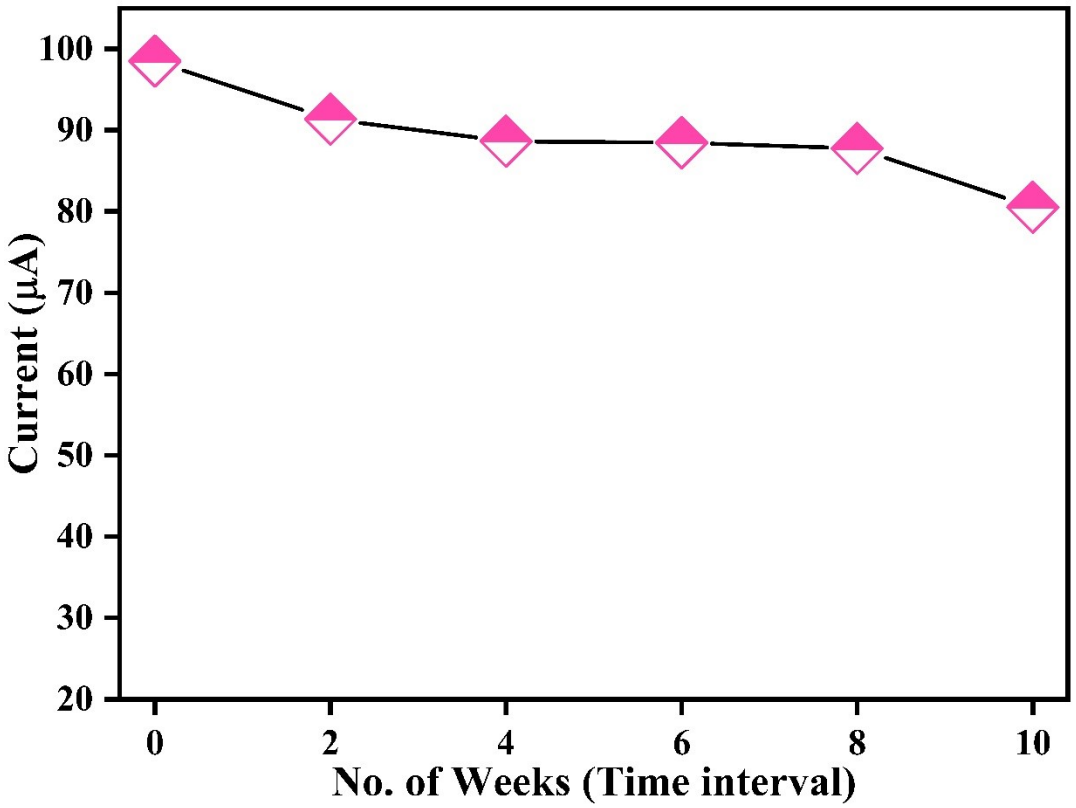

Fig.S4: Stability of immunoelectrode

S8 Artificial Saliva Analysis

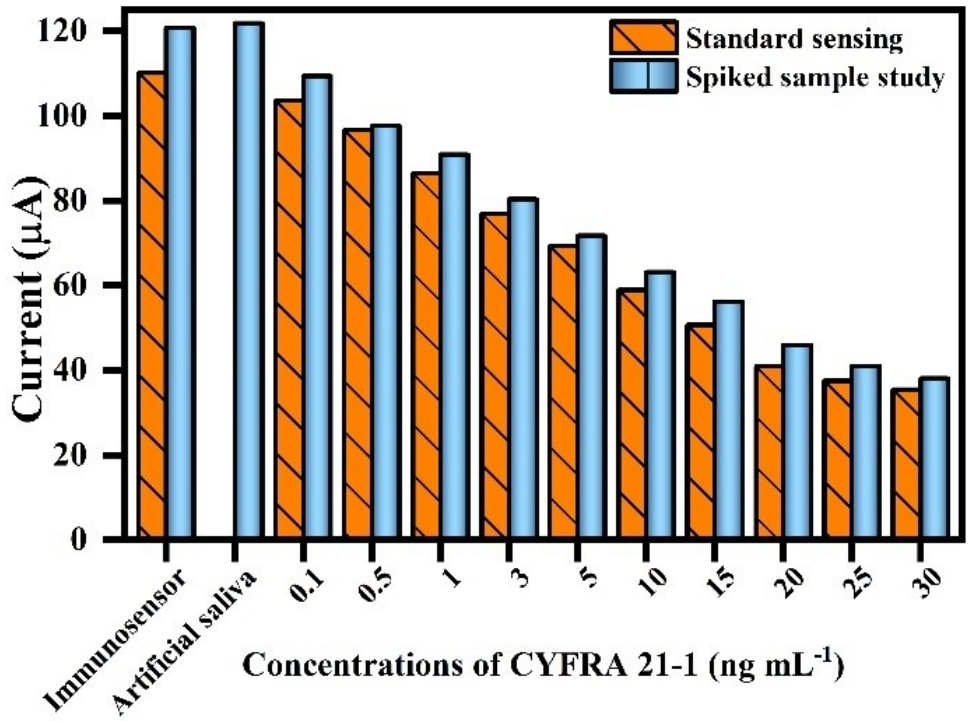

Fig. S5: Comparative evaluation of current response with %RSD and %recoveries using the developed BSA/anti-CYFRA-21-1/L-cyst@MNPs/Ti_3C_2-MXene/GSPE immunosensor between spiked sensing and standard sensing current values

References

1 D. Verma, S. Z. H. Hashmi, G. Lakshmi, R. K. Sajwan, A. Kumar and P. R. Solanki, *Microchem. J.*, 2023, 108964.

2 R. Ospina and F. Marmolejo-Ramos, *Front. Appl. Math. Stat.*, 2019, **5**, 43.